

Quadcopter Sound Characterization using a UAV Test Stand

Jared Schmal¹
D. W. Herrin²
University of Kentucky
151 Ralph G. Anderson Building
Lexington, KY 40506-0503
USA

Daniel Fernández Comesaña³
Microflown Technologies
Tivolilaan 205
6824 BV Arnhem
The Netherlands

ABSTRACT

Unmanned Aerial Vehicles (UAVs) generate a complex acoustic field that is not entirely understood. Many components and their interactions contribute to the overall noise level and behavior of the acoustic field. A UAV test stand configured to emulate a small quadcopter with a wheelbase of 61 cm was used to determine the acoustic response of a multicopter. Microflown Technologies Scan & Paint 3D solution was utilized to obtain sound pressure, particle velocity, and sound intensity measurements close to the source, along with propagation planes for three-dimensional visualizations containing both amplitude and direction. Draw away measurements using a PU probe were also completed to analyze the sound field characteristics further from the source. The number of propellers in operation was varied to determine the impact of adding additional sources. Aeroacoustic sources, near and far field behavior, interaction noise, directivity, and the sound field propagation of each case is discussed.

1. INTRODUCTION

The rapid development of Unmanned Aerial Vehicles (UAVs) over the past ten years has generated a booming market in the recreational, commercial, and military sectors. These vehicles have been designed for a myriad of applications, such as photography and film, surveying and mapping, infrastructure inspections, package delivery, search and rescue, and agricultural spraying. The adoption and utilization of UAVs continue to grow as new and innovative uses are discovered. Vibro-acoustics has been a research and development focus, and this is expected to continue well into the future as noise pollution is a major hurdle for public acceptance of UAVs.

Most experimental research on UAVs to date has focused on sound pressure measurements in the far field using microphones. While the acoustic signature and sound power levels of UAVs are now generally understood and accepted, little is currently known about the near field acoustic behavior. In this paper, sound pressure and particle velocity measurements were completed using a UAV test stand to characterize the near and far field behavior of a quadcopter.

¹ Email: jared.schmal@uky.edu

² Email: david.herrin@uky.edu

³ Email: fernandez@microflown.com

2. BACKGROUND

UAVs generate a complex acoustic field that is not entirely understood. Many components and their interactions contribute to the overall noise level and directionality of the acoustic field, but in most cases, the primary acoustic source is generated by the propellers [1]. Propeller noise contains discrete components that generate tonal noise and continuous components that generate broadband noise [2]. Tonal noise is produced by steady or unsteady periodic source mechanisms, while broadband noise is produced from unsteady random source mechanisms. The tonal response of a propeller mainly occurs at the blade pass frequency (BPF) and its harmonics, which are defined as

$$f_{BPn} = \frac{nNR}{60} \text{ [Hz]}, \quad (1)$$

where n is an integer, N is the number of blades, and R is the revolutions per minute of the motor shaft [3]. Propeller noise can be categorized into three primary sources: thickness noise, loading noise, and nonlinear noise [2]. Thickness and loading sources are relevant to UAVs, but nonlinear sources are only a factor for propellers approaching or exceeding supersonic speeds and are therefore neglected in this analysis. Thickness noise is caused by the periodic displacement of flow over the blades and acts like a monopole source. Thickness noise is usually a discrete component, generating a tonal response that is primarily dependent on the propeller tip speed and becomes more significant as the propeller velocity increases. The airfoil shape, blade cord, and blade thickness are also variables related to thickness noise. Loading noise can be steady and random, generating both tonal and broadband components, and can be quantified as a dipole source. The tonal component of loading noise is caused by periodic pressure fluctuations acting on the blade surface and are the same forces that generate lift and drag. Broadband loading noise is due to atmospheric turbulence or wake turbulence, caused by flow interactions from the airframe that are ingested back into the propeller stream. The airframe can be an important acoustic source due to interactions between the propeller and quadcopter arm, producing both tonal and broadband noise that is dependent on the receiver's location [4]. The phase of these sources can differ, leading to constructive and destructive interference, generating a highly directive and complex acoustic field [2].

The decay rate of a sound field can be used to classify sources. A monopole can be viewed as an omni-directional pulsating sphere. The decay rate of a monopole for sound pressure and particle velocity is r^{-1} , regardless of the distance from the source. Dipole sources are more complex and decay at different rates in the near field. The sound pressure of a dipole is defined as

$$p_{\text{dipole}} = \mathbf{D} \cdot \hat{\mathbf{e}}_r \left(\frac{ik}{r} + \frac{1}{r^2} \right) e^{-ikr}, \quad (2)$$

where \mathbf{D} is the dipole moment vector, $\hat{\mathbf{e}}_r$ is the unitary vector from the field point to the origin, i is the imaginary number, k is the wavenumber, and r is the distance to the source [5]. The wave number can then be defined as

$$k = \frac{\omega}{c} \quad (3)$$

where ω is the angular frequency and c is the speed of sound. In the near field, sound pressure decays at a rate of r^{-2} , which equates to 12 dB when the distance from the source is doubled. The particle velocity of a dipole is defined as

$$\mathbf{V}_{\text{dipole}} = \frac{\mathbf{D} \cdot \hat{\mathbf{e}}_r}{\rho_0 \omega} \left(\frac{ik^2}{r} + 2 \frac{k}{r^2} - \frac{2i}{r^3} \right) (e^{-ikr}) \hat{\mathbf{e}}_r, \quad (4)$$

where ρ_0 is the ambient density. In the near field, particle velocity decays at two different rates, r^{-2} and r^{-3} , equating to 12 and 18 dB for each doubling of the distance from the source. The boundary between the near and far field can be difficult to define depending on the source, but generally the near field can be defined as

$$kr \ll 1, \quad (5)$$

where k is the wave number and r is the distance from the source [3]. The far field can then be estimated at values where $kr \geq 1$.

3. MEASUREMENT SETUP

A UAV test stand was configured to emulate a quadcopter with a wheelbase (diagonal length between each motor rotor) of 61 cm [6]. XRotor 40A electronic speed controllers (ESCs), T-Motor MN3508 brushless electric direct current (BLDC) motors and 38.1 cm foldable carbon composite propellers were utilized. The stand was powered by two DC power supplies that simulate a six-cell battery pack with a nominal voltage of 22.2 V. A computer was used to send commands to an Arduino Mega 2560 micro controller that allows each motor to be controlled and monitored independently. The Arduino sends pulse width modulation (PWM) signals to the ESCs as well as powers and records sensor information. The current input and the revolutions per minute (RPM) of each propeller were individually monitored using hall effect and infrared (IR) sensor modules.

All measurements were conducted in the hemi-anechoic chamber located at the University of Kentucky. The chamber dimensions are 6.1 m \times 6.1 m \times 3.0 m and meets the ISO requirements for acoustic testing at 150 Hz and above. Hovering conditions were assessed with each motor operating at approximately 3500 RPM producing a stationary signal for the duration of the measurements. This allowed for scanning methods and frequency averaging to be used for spectral analysis. The number of propellers in operation was varied to determine the impact of adding additional sources. Two types of measurements were used to access the acoustic behavior of the UAV test stand.

3.1. Scan&Paint 3D

The Microflow Scan&Paint 3D solution is a portable measurement tool capable of visualizing an acoustic field in three-dimensions [7]. The equipment can be seen in Figure 1 and is described below.

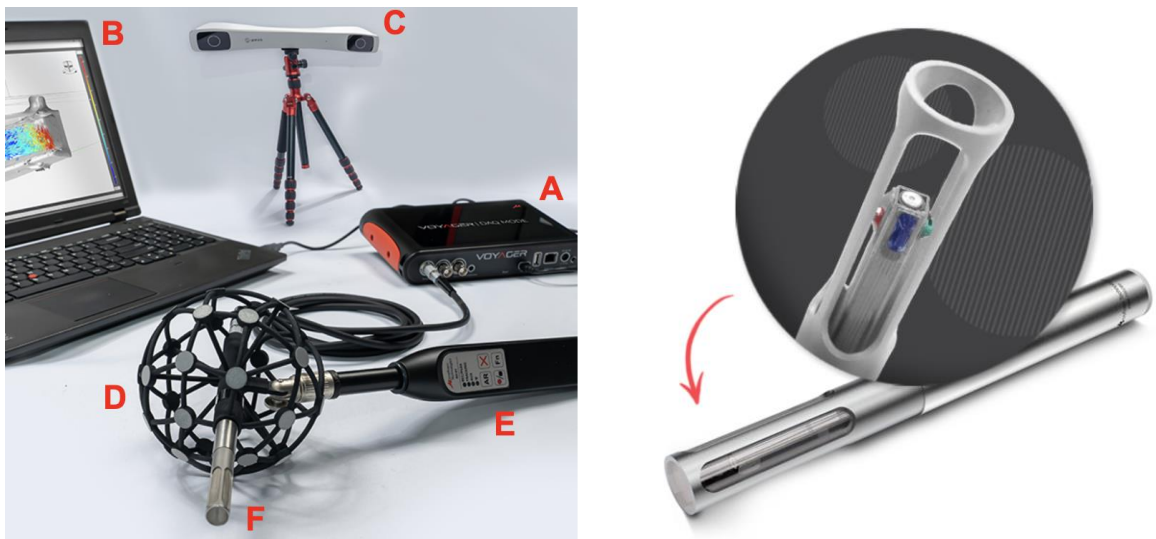


Figure 1: Microflow Scan&Paint 3D solution (left) and 3D sound intensity probe (right).

- A. Microflown Voyager - A portable NVH analyzer and data acquisition system (DAQ)
- B. Laptop with Scan&Paint 3D software (Velo)
- C. PST Iris optical tracking camera
- D. Tracking sphere containing randomly spaced reflectors.
- E. Remote for single user measurement control
- F. Microflown 3D sound intensity probe (Frequency range 20 Hz – 10 kHz)

The 3D sound intensity probe is manually roved along the measurement surface as the recorded signals and position are synchronized in real-time. The sound field is then discretized into a cuboid grid over a 3D model of the object under test with a 1 cm cell resolution. The direction (sound intensity and particle velocity vectors) and magnitude of the sound field can then be calculated using the discretized sound pressure and orthogonal particle velocity signals [8]. For this research, the sound intensity probe was manually roved along the top and bottom propeller planes, approximately 5 cm from the propeller surface, to analyze the near field behavior. In addition, vertical propagation planes extending from the center of the test stand were captured at multiple angles. Two examples of captured measurement paths can be seen in Figure 2.

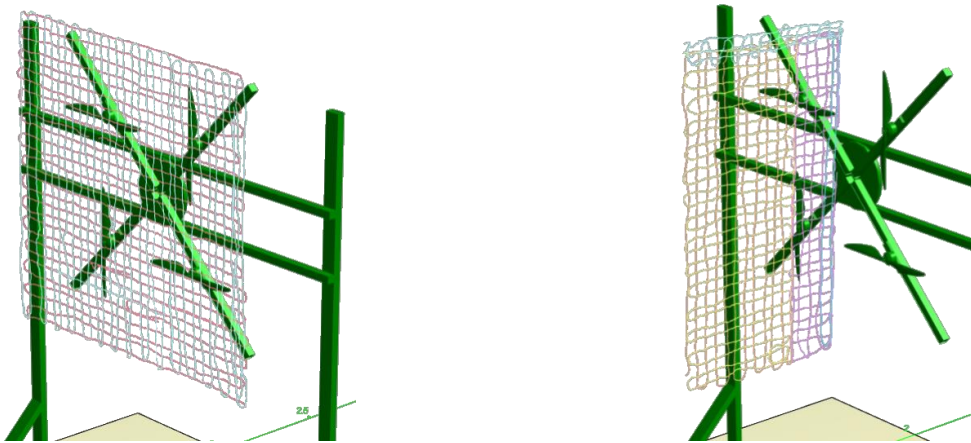


Figure 2. Sound intensity scanning paths: Top plane (left) and 90° propagation plane (right).

3.2. Draw Away Measurements

Draw away measurements were completed to determine directionality and decay rate. This was completed using a Microflown PU probe to obtain both the sound pressure and particle velocity at the same point in space. Two propagation planes and seven distances from the test stand were measured, doubling the distance from each point, as shown in Figure 3. The maximum distance that could be measured was limited by the dimensions of the anechoic chamber. The measurement height was selected to avoid obstructions on the bottom side of the test stand for the 5 and 10 cm positions. Captures were recorded for thirty seconds and then averaged in the frequency domain.

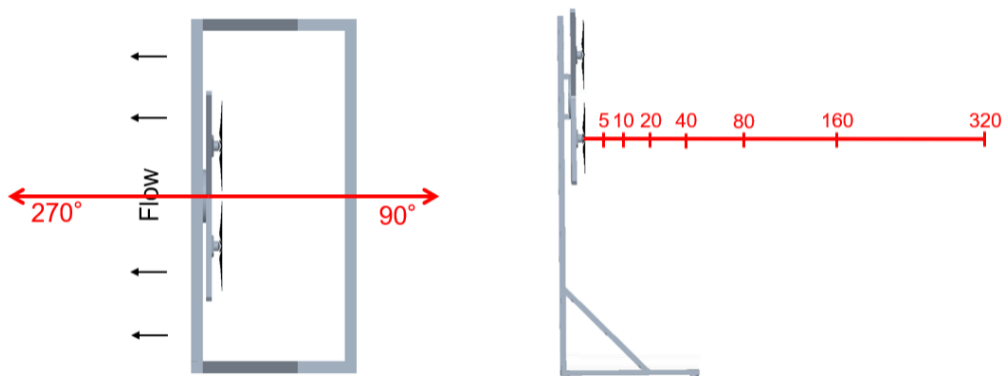


Figure 3. Draw away measurement locations (cm).

4. RESULTS

A single propeller was measured running at a constant speed of approximately 3,500 RPM. The arm of the test stand was rotated in the vertical position and the motor mount was positioned towards the end of the arm, limiting interaction with the test stand frame. The volume around the operating propeller was scanned using the Microflow Scan&Paint 3D solution. All results shown below are A-weighted, unless otherwise stated.

The active sound intensity is plotted in Figure 4 from 100 to 10,000 Hz for the top, propeller, and bottom planes. The directivity of the sound field is perpendicular to the propeller axis, with the sound dissipating rapidly in the propeller plane. The propagation and magnitude of the acoustic field can be surmised using the vector nature of sound intensity. The acoustic behavior in the near field corresponds to the rotational direction of the propeller, but transitions to propagate normal to the source as the distance is increased. The scanning measurements of the top plane result in a toroid shape around the center of the propeller that is caused by the dipole source spinning around the propeller axis. Whereas turbulence caused by flow or interactions from the arm are likely causing interference on the bottom plane, therefore fragmenting the typical dipole pattern.

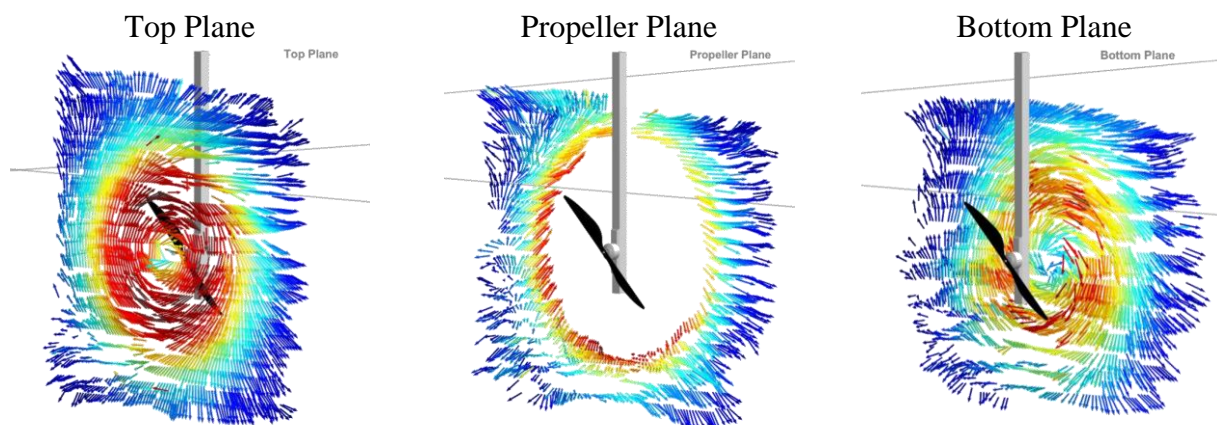


Figure 4. Broadband sound intensity of a single propeller on the test stand.

The active sound intensity at 120 Hz (BPF) along a propagation plane perpendicular to the center of the propeller is seen in Figure 5. At this low frequency, the dipole behavior is clearly visualized. It is important to note that flow effects in the measurement can be seen in the bottom propagation plane.

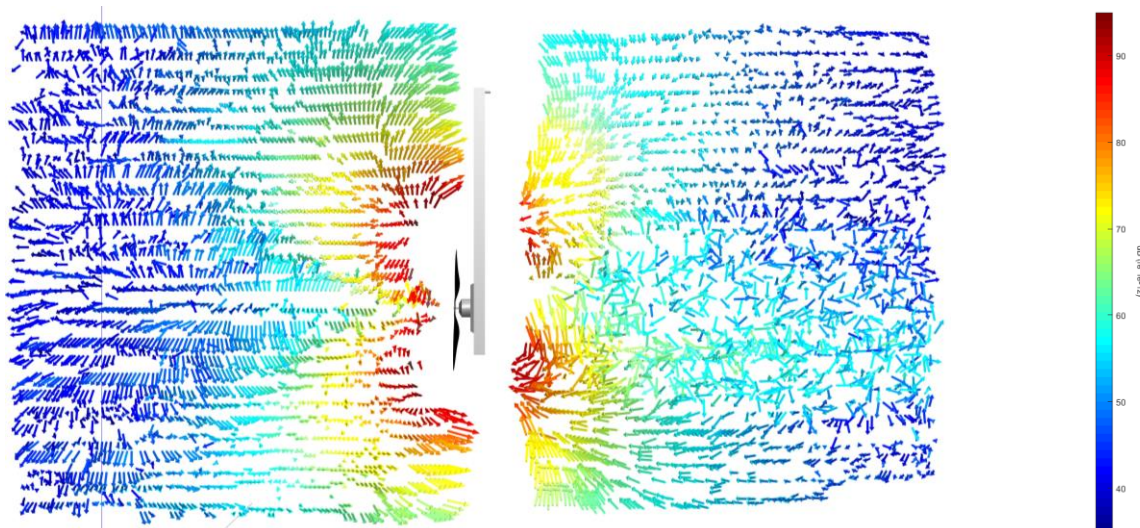


Figure 5. Sound intensity at 120 Hz (BPF) along a propagation plane perpendicular to the center of the propeller.

The active sound intensity of the BPF along a propagation plane at a 45° angle to the center of the propeller is seen in Figure 6.

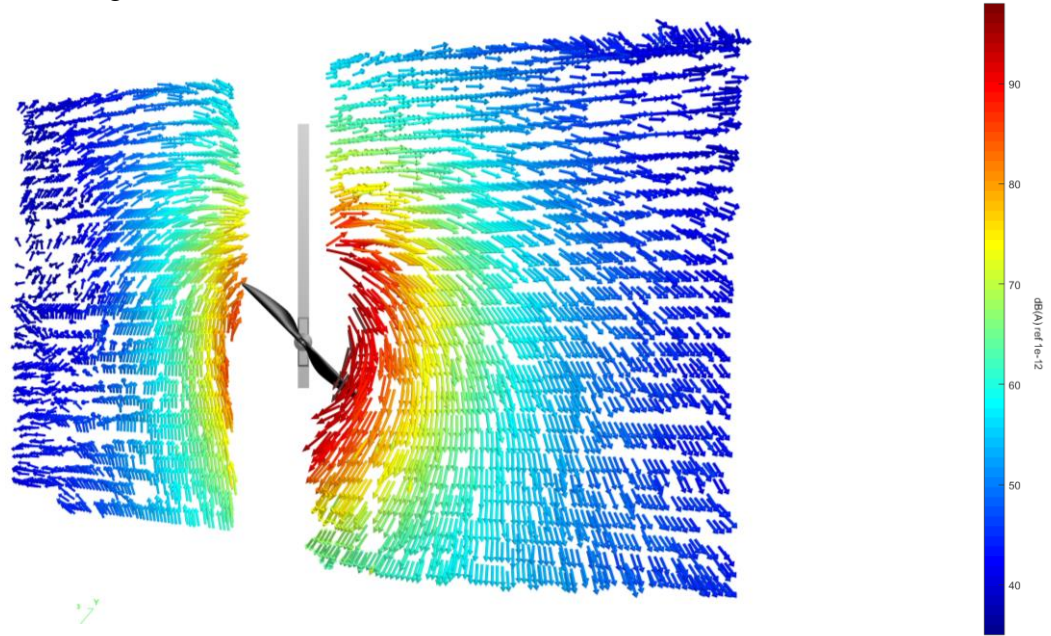


Figure 6. Sound intensity of the BPF along a 45° propagation plane from the center of the propeller.

Sound intensity colormaps of the plane normal to the propeller axis are visualized in Figure 7. A frequency analysis is shown with the BPF and two high amplitude peaks at 2484 Hz and 3328 Hz. The dipole behavior of the BPF is observed while the higher frequency plots appear to be spherical, acting like a monopole. Once again, the turbulence can be visualized for all frequencies on the back side of the propeller. At the higher frequencies, additional noise is observed behind the quadcopter arm.

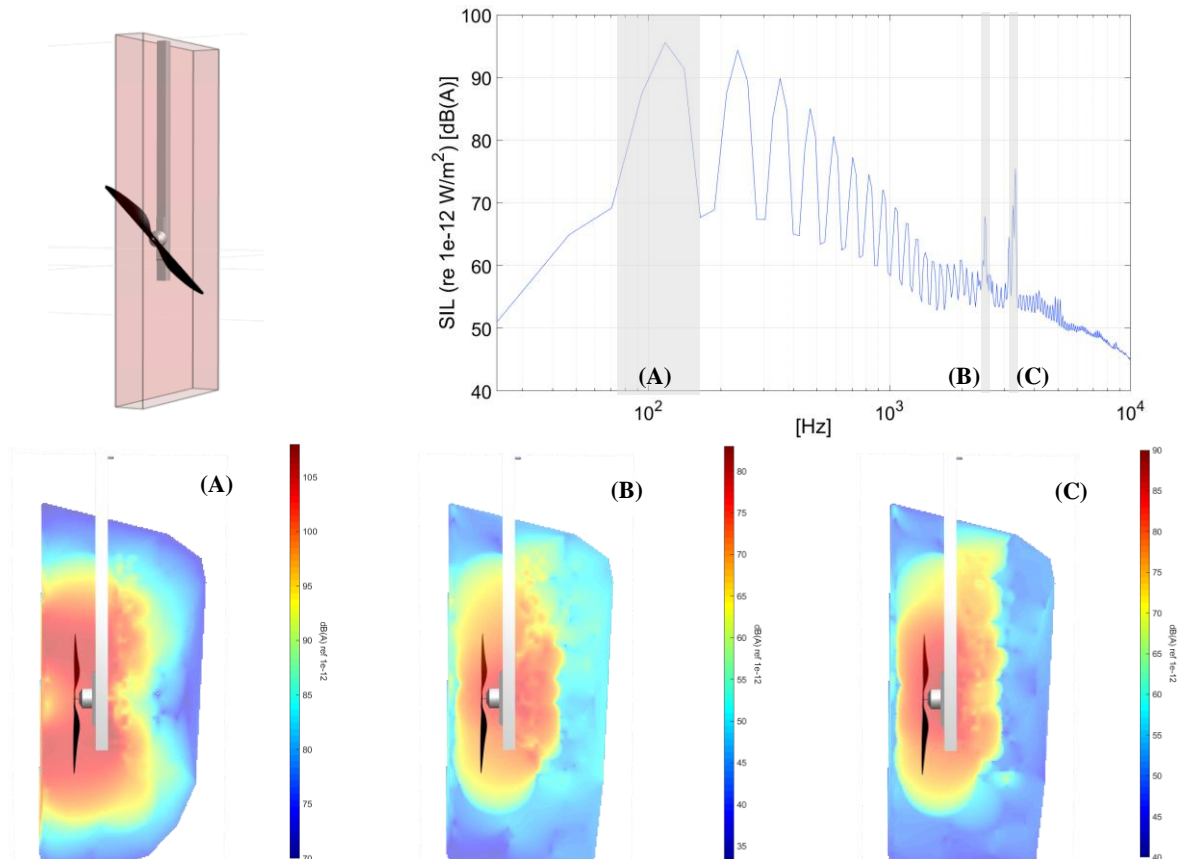


Figure 7. Sound intensity frequency analysis: 120 Hz (left), 2484 Hz (center), and 3328 Hz (right).

The sound intensity on the top plane as the number of propellers in operation is varied is shown in Figure 8. Although interactions do occur at the blade tip boundaries when additional propellers are in operation, the acoustic behavior of the extra sources appears to remain unchanged. It should be noted that the direction of the sound intensity field over each propeller matches the rotation direction in all 4 operational cases.

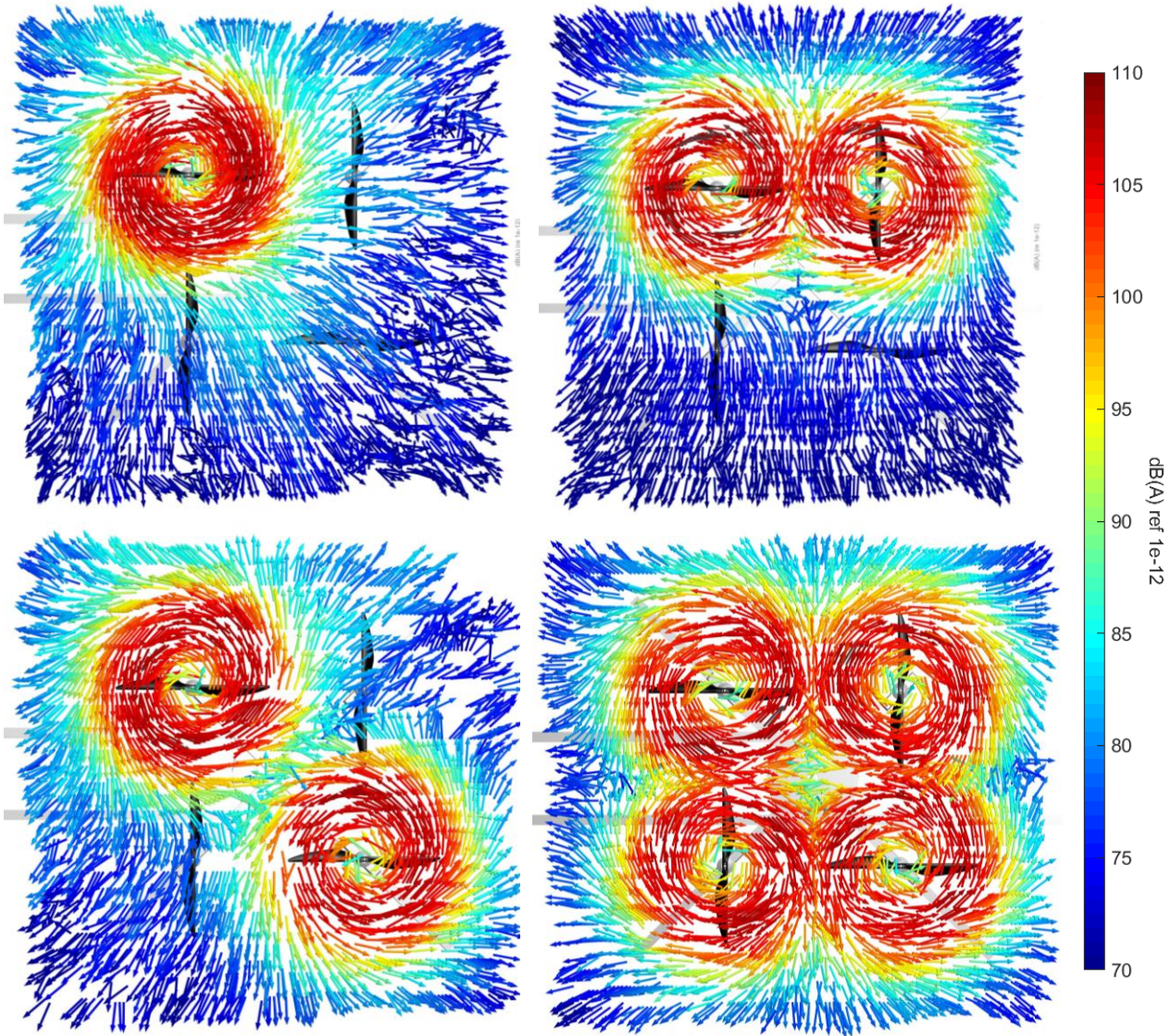


Figure 8. Sound intensity on the top plane as the number of propellers in operation varies.

Huanxian et al. performed an extensive study on a dual propeller testing rig and discovered radiated noise of the propeller pair could be predicted using superposition [9]. Assuming the sources in Figure 8 are uncorrelated, the overall sound power level was calculated using the superposition principle.

Sound power from the single propeller case (top left) was used to estimate the addition of propeller sources. The measured versus calculated overall sound power level of the top plane as the number of propellers in operation is varied is plotted in Figure 9. The results correspond well, indicating that the sources are indeed uncorrelated and hence the sound emission from multiple propellers can accurately be predicted using sound power measurements of a single unit.

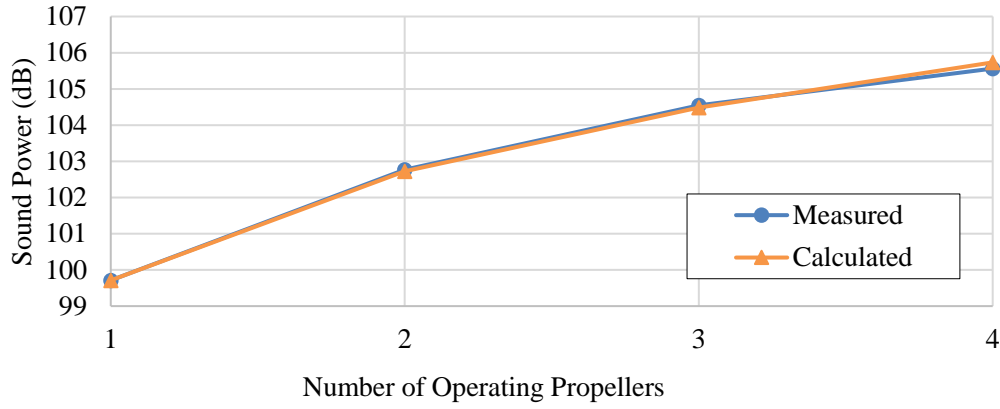


Figure 9. Measured and calculated sound power level of top plane as the number of propellers in operation is varied.

Colormaps of the top and bottom propeller planes from 100 Hz to 10 kHz are shown in Figure 10.

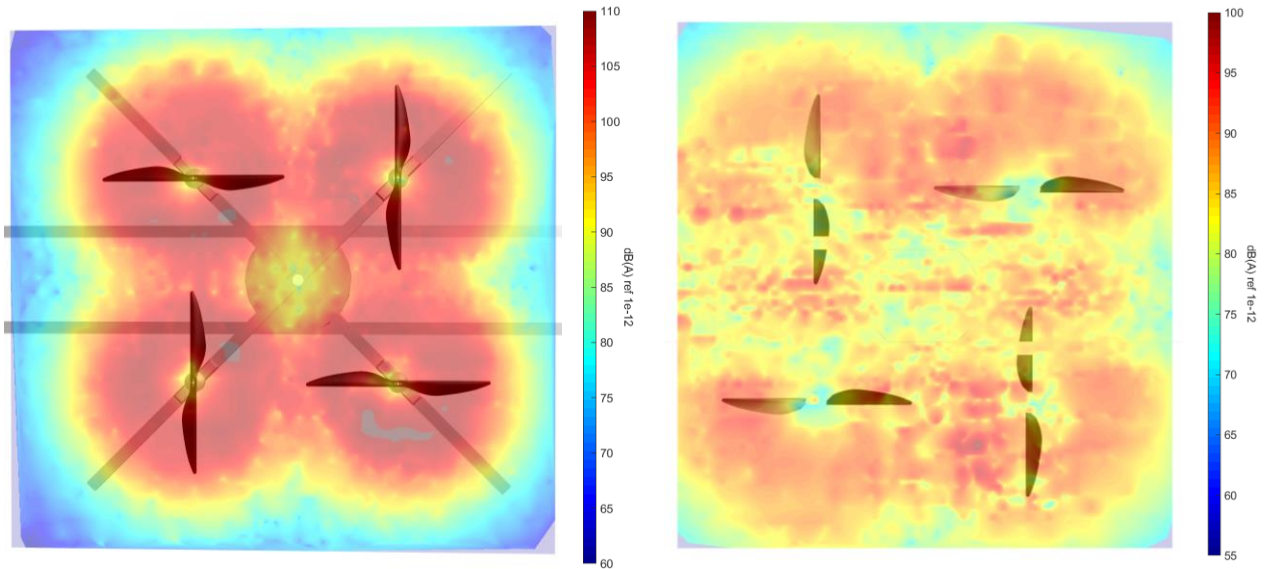


Figure 10. Broadband sound intensity of top and bottom propeller plane.

The sound intensity of the BPF at planes located 5, 10 and 20 cm from the top propeller surface are shown in Figure 11. The toroid pattern caused by the dipole source dissipates rapidly as the distance from the propellers is increased. The sound field is fragmented, with the highest amplitudes between the blade tips, at the 20 cm plane.

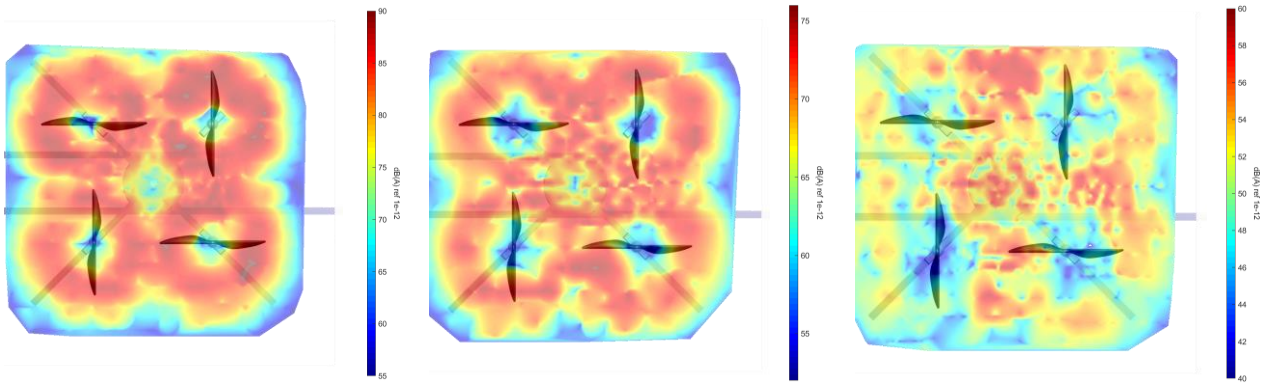


Figure 11. Sound intensity of BPF top plane (5, 10, and 20 cm from top of propeller surface).

The sound intensity at the same frequency range (120 Hz, at BPF) along a propagation plane perpendicular to the center of the test stand is seen in Figure 12.

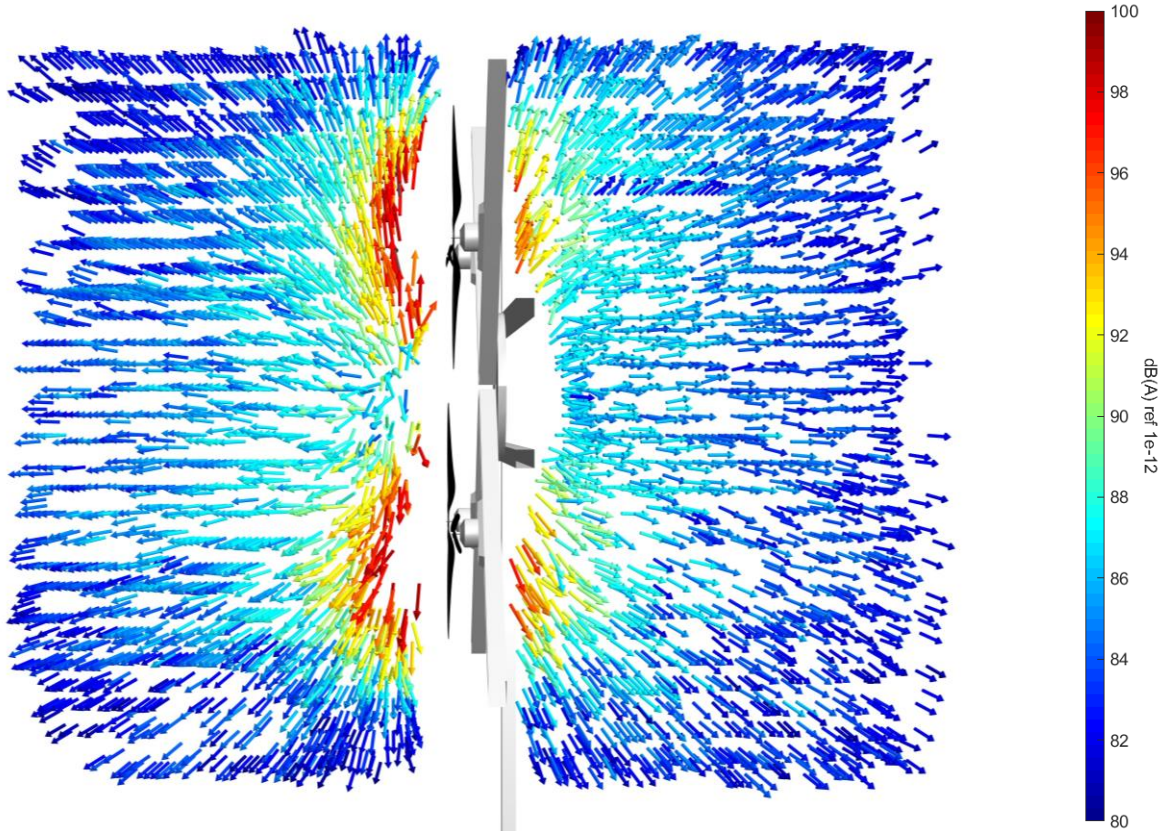


Figure 12. Sound intensity along a propagation plane perpendicular to the center of the test stand.

Particle velocity and sound pressure draw away measurements are plotted against the wave number multiplied by the distance from the source (kd) in Figure 13, enabling an analysis of the results in terms of wavelength. The 125 Hz third octave band containing the BPF is plotted. Three rates of decay can be observed with particle velocity in both propagation planes. For the top plane (90-degree line shown in Figure 3), a rate of 10 dB for each doubling of distance begins when kd equals 0.23, 22 dB when kd equals 0.47, and 7 dB when kd equals 1.86. As expected, the particle velocity decay rate converges to the same rate as sound pressure once the far-field is reached. For the bottom (270-degree), flow side, the decay rate is reduced and particle velocity does not converge with sound pressure. This is likely caused by flow-induced noise in the measurements.

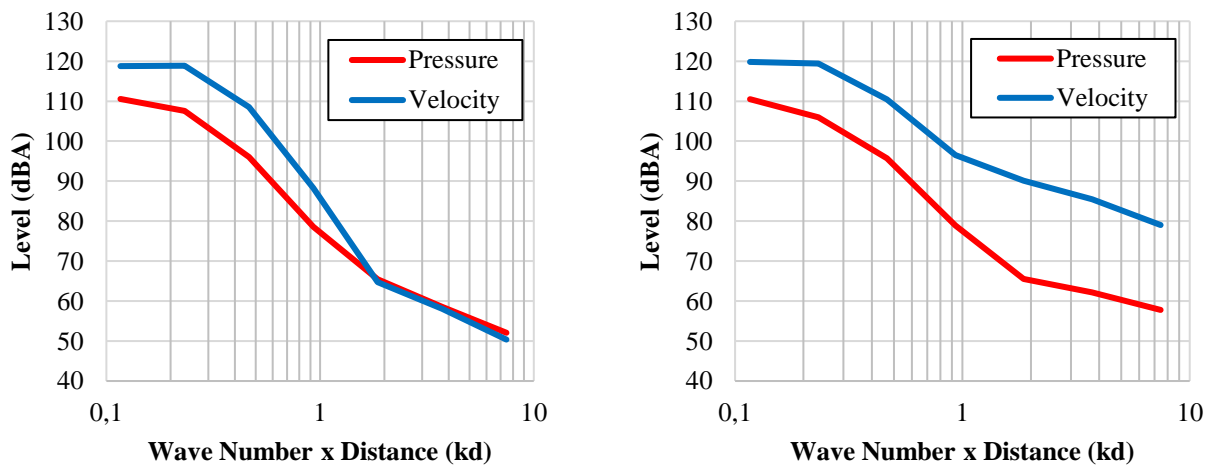


Figure 13. Draw away measurements of the 125 Hz third octave band along the 90-degree (left) and 270-degree (right) propagation planes.

5. CONCLUSIONS

Sound intensity measurements were completed on a UAV test stand in a quadcopter configuration. Two types of measurements were completed: 3D sound intensity scans using Microflown Scan&Paint 3D and draw away tests using a 2D sound intensity probe. All measurements were performed when the stand was operating at approximately 3500 RPM, simulating a hovering quadcopter and producing a stationary sound field. The near field behavior of the top, suction side, and bottom, flow side, of the UAV test stand was analyzed. Strong dipole patterns were revealed on the top side of the quadcopter while turbulence due to flow effects and propeller-structure interactions likely cause the fragmentation on the bottom side. The active sound intensity in the vicinity of the blades follows the rotational direction of the propeller, then transitions to propagate normal to the source. The number of propellers in operation was varied to determine the impact of adding additional sources and minimal interaction noise was discovered. The propeller sources were shown to be uncorrelated, enabling superposition to be used for analytical models. Draw away tests were completed and behavior similar to dipole source theory was observed for the third octave band containing the blade pass frequency.

ACKNOWLEDGEMENTS

The authors gratefully acknowledge the support from the Vibro-Acoustics Consortium and Microflown Technologies.

REFERENCES

- [1] N. Intaratap, W. N. Alexander, W. J. Devenport, S. M. Grace, and A. Dropkin, "Experimental Study of Quadcopter Acoustics and Performance at Static Thrust Conditions," in *The 22nd AIAA/CEAS Aeroacoustics Conference*, Lyon, France: American Institute of Aeronautics and Astronautics, 2016.
- [2] M. J. Crocker, Ed., *Handbook of Noise and Vibration Control*. Hoboken, N.J: John Wiley, 2007.
- [3] M. J. Crocker and J. P. Arenas, *Engineering Acoustics - Noise and Vibration Control*. Wiley, 2021.
- [4] N. S. Zawodny and D. D. Boyd, "Investigation of Rotor–Airframe Interaction Noise Associated with Small-Scale Rotary-Wing Unmanned Aircraft Systems," *Journal of the American Helicopter Society*, vol. 65, no. 1, pp. 1–17, 2020.
- [5] J. H. Ginsberg, *Acoustics-A Textbook for Engineers and Physicists: Volume I: Fundamentals*. Springer International Publishing, 2018.
- [6] J. Schmal, D. Herrin, and D. F. Comesaña, "Development of a UAV Test Stand," in *52nd International Congress and Exposition on Noise Control Engineering*, Japan, 2023.
- [7] "Scan&Paint 3D | Visualizing 3D Sound Intensity," *Microflown Technologies*. <https://www.microflown.com/products/sound-localization-systems/scan-paint-3d>
- [8] D. F. Comesanã, S. Steltenpool, M. Korbasiewicz, and E. Tijs, "Direct Acoustic Vector Field Mapping: New Scanning Tools for Measuring 3D Sound Intensity in 3D Space," presented at the EuroNoise, 2015.
- [9] H. Bu, H. Wu, C. Bertin, Y. Fang, and S. Zhong, "Aerodynamic and Acoustic Measurements of Dual Small-Scale Propellers," *Journal of Sound and Vibration*, vol. 511, p. 116330, Oct. 2021.